Arch. Metall. Mater. **71** (2026), 2, 541-544

DOI: https://doi.org/10.24425/amm.2026.158837

BYOUNGYONG IM[1,2], JIWON CHOI[1], KI BUEM KIM[2], DAE-GUEN KIM[1*]

MICROSTRUCTURE EVOLUTION OF NICKEL STRIKE PLATING LAYER BY ELECTROCHEMICAL DEPOSITION AND HEAT TREATMENT

Nickel strike layers were electrodeposited on stainless steel from a $NiCl_2$-HCl bath, and the effects of applied potential, deposition time, and post-plating heat treatment were investigated. Chronoamperometry showed that cathodic current density increased and current fluctuations became more pronounced at more negative potentials, indicating intensified hydrogen evolution. Surface images revealed needle-like morphology at less negative potentials, whereas non-uniform deposition with incomplete coating regions appeared at –1.8 V due to competition from hydrogen evolution. Heat treatment transformed the surface into polygonal grains and promoted grain coarsening. Texture analyses indicated increased average grain size and decreased local misorientation, suggesting microstructural recovery and relaxation of residual/internal stress.

Keywords: Nickel; Strike Plating; Heat treatment; Electrochemical deposition

1. Introduction

Surface modification by electrodeposition is widely used to add corrosion resistance, wear resistance, and functional surface properties to structural metals used in industrial components. Strike plating is a short, initial electrodeposition step that deposits a thin, highly active, and adherent metal layer to enable subsequent plating. Nickel is commonly used as the material for the strike layer, and its bath chemistry and electrical conditions can be tuned to control deposit microstructure and properties [1-6].

Strike plating on stainless steel uses a Woods strike bath containing HCl (10 vol.%) and $NiCl_2$ (240 g/dm^3) operated at high current density for a short time [7]. For comparison, a Watts nickel bath platform uses $NiSO_4 \cdot 2O$ (260 g/dm^3), $NiCl_2 \cdot 6H_2O$ (50 g/dm^3), and H_3BO_3 (30 g/dm^3) [4,8,9]. In the electrolyte, NiSO4 and $NiCl_2$ supply Ni^{2+}, chloride increases conductivity and supports nickel anode dissolution, and boric acid acts as a buffer to limit local pH rise and help prevent $Ni(OH)_2$ precipitation near the cathode.

Nickel electrodeposition research has been conducted to control microstructure and properties by adjusting bath composition (including additives), operational conditions (temperature, stirring) and electrical control modes (potential control, current control, pulse mode) [1,2,5,9]. Many studies on electrodeposition have focused on controlling morphology [1,10]. However, to ensure the desired mechanical properties of electrodeposited layers, investigations of crystallographic transitions and internal stress are required [5,11]. Moreover, electrodeposited nickel microstructure is not necessarily stable; heat-treatment of deposits is considered to modify microstructure and relieve internal stress generated during electrodeposition [12,13].

Therefore, this study aims to optimize nickel strike plating conditions to enhance morphological stability and to investigate the effect of post-plating heat treatment on the deposited film. To achieve this, we control the applied potential and deposition time during nickel strike electrodeposition and evaluate post-heat-treatment changes through microstructural characterization.

2. Experimental

A 500 mL nickel strike bath was prepared by dissolving 1.05 M $NiCl_2 \cdot 6H_2O$ (Alfa Aesar) and adding 1.17 M HCl (DAEJUNG) to deionized water. The electrolyte was stirred for 30 min. Electrochemical experiments were conducted in a three-electrode cell using a potentiostat (AUTOLAB, PGSTAT302N). An Ag/AgCl electrode was used as the reference electrode, and pure nickel metal was used as the counter electrode. Nickel was electrodeposited onto stainless steel 316 plates that had been polished with #2000 SiC paper, cleaned with ethanol, and rinsed

[1] MATERIALS SCIENCE AND CHEMICAL ENGINEERING CENTER, INSTITUTE FOR ADVANCED ENGINEERING (IAE), YONGIN, REPUBLIC OF KOREA
[2] SEJONG UNIVERSITY, SEOUL, DEPARTMENT OF NANOTECHNOLOGY AND ADVANCED MATERIALS ENGINEERING, REPUBLIC OF KOREA

* Corresponding author: dgkim@iae.re.kr

with deionized water. Prior to nickel strike electrodeposition, the stainless-steel surface was activated in 10 vol.% HCl for 30 s to remove the passive oxide film. A Teflon housing was used to expose a fixed 1 cm^2 area of the stainless-steel surface to the electrolyte. To investigate the electrochemical behavior of nickel plating, chronoamperometry was performed at –0.9, –1.2, –1.5, and –1.8 V vs. Ag/AgCl for 10 min at each potential. All experiments were performed at room temperature with continuous stirring.

After electrodeposition, samples with electrodeposited Ni films were rinsed several times with deionized water to remove residual electrolyte and then dried in a vacuum oven for 24 h. Subsequently, the dried samples were heat-treated at 300 ~ 900°C under an argon atmosphere using a tube atmosphere furnace. The samples were heated to the target temperature at a heating rate of 10°C/min, held for 3 h, and then furnace-cooled under an argon atmosphere.

Phase identification and morphology of the samples were characterized by X-ray diffraction (XRD; Shimadzu, XRD-6100) and field-emission scanning electron microscope (FE-SEM; Hitachi, SU8700), respectively the average surface roughness (R_a) was measured using a 3D Laser Confocal Surface Profiler (KEYENCE, VK-X3000).

3. Results and discussion

Fig. 1(a) shows current transient curves with respect to each applied reduction potential. As the applied potential becomes more negative (from –0.9 to –1.8 V vs. Ag/AgCl) the cathodic current density increases in magnitude, indicating a higher overall reduction rate during electrodeposition. At –0.9 and –1.2 V the current density is comparatively stable and exhibits only small fluctuations. However, at more negative potentials (–1.5 and especially –1.8 V), the current transient curves show large and irregular fluctuations. This behavior is typically attributed to hydrogen evolution and bubble dynamics at the cathode; intermittent bubble nucleation, growth, and detachment transiently block and re-expose the cathode surface and locally change electrolyte resistance, producing current noise. Hydrogen evolution reduces current efficiency and can adversely affect surface morphology, for example by producing rough deposits.

XRD patterns were analyzed to identify the phases of all samples. Fig. 1(b) shows the XRD patterns of the deposits on stainless steel. The diffraction peaks were indexed to Ni (electrodeposited layer) and γ-Fe (stainless-steel substrate). As the applied potential became more negative, the Ni peaks increased in intensity relative to the γ-Fe peaks. This trend is attributed to an increased deposit thickness at more negative potentials.

Fig. 2(a, b) show top-view SEM images of nickel layers electrodeposited on stainless steel. The deposits exhibit a needle-like morphology, and the feature size increases as the applied potential becomes more negative. In the range of –0.9 to –1.5 V, the nickel layers show relatively uniform surface coverage. By contrast, at –1.8 V, areas of incomplete nickel coverage are observed, indicating non-uniform deposition. This behavior is attributed to intensified hydrogen evolution at the more negative potential. As a result, the nickel layer roughness increases due to deposit growth and hydrogen evolution, and the Ra value reaches 38 nm at –1.8 V. Fig. 2(c) shows cross-sectional SEM images of the nickel layers. The measured thicknesses of the nickel layers were 4.6 (–0.9 V), 5.4 (–1.2 V), 8.3 (–1.5 V), and 10.3 μm (–1.8 V), increasing with more negative applied potentials. The theoretical thicknesses, calculated from the current transient curves in Fig. 1(a) using Faraday's law, were 20.5 (–0.9 V), 24.6 (–1.2 V), 56.4 (–1.5 V), and 95.5 μm (–1.8 V). Accordingly, the current efficiencies were 22.3% (-0.9 V), 22.0% (–1.2 V), 14.7% (–1.5 V), and 10.8% (–1.8 V), decreasing as the potential became more negative. The discrepancy between the measured and theoretical thicknesses is attributed to competitive hydrogen evolution, which becomes more significant at more negative potentials.

Nickel strike plating experiments were conducted with varying deposition times at –0.9 V, where hydrogen evolution was low and deposition was stable. The thickness of the nickel layer increased with deposition time (1.9 μm at 5 min, 4.7 μm at 10 min, 8.2 μm at 20 min, and 15.4 μm at 30 min), with an average growth rate of approximately 0.47 μm/min.

Samples prepared at –0.9 V for 10 min were used to investigate the effect of heat treatment. Fig. 3(a) shows top-view SEM images of the nickel layers after heat treatment at different temperatures. With increasing heat-treatment temperature, the surface morphology evolves from a needle-like (acicular) structure to a polygonal, faceted grain morphology, indicating microstructural coarsening and recrystallization-driven grain

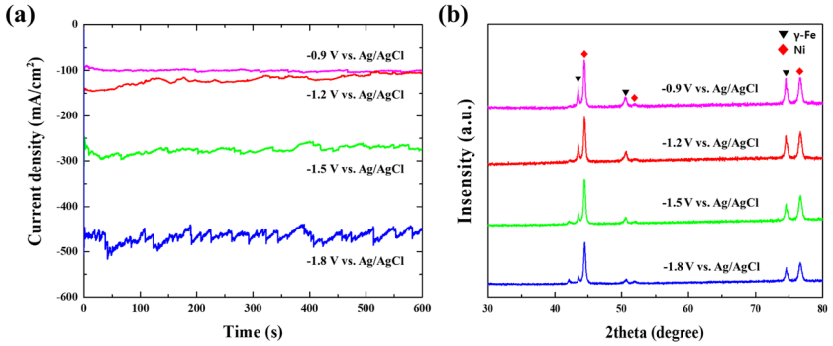

Fig. 1. (a) Current density-time transient curves recorded during Ni strike electrodeposition on stainless steel at different applied potentials. (b) XRD patterns of the corresponding nickel-coated stainless-steel samples

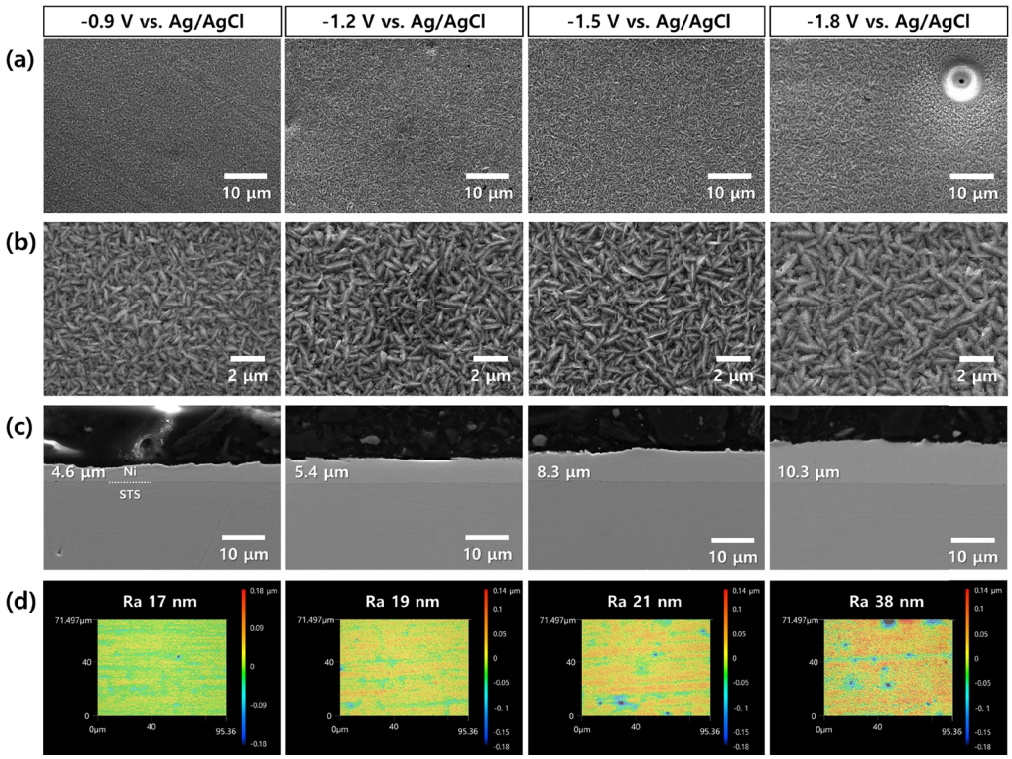

Fig. 2. Surface and cross-sectional characterization of Ni layers electrodeposited on stainless steel at different applied potentials: (a) low-magnification top-view SEM images, (b) high-magnification top-view SEM images, (c) cross-sectional SEM images showing coating thickness, and (d) 3D surface-profiler images with Ra values

growth. This morphological transition is consistent with thermally activated diffusion and grain-boundary migration during annealing, which promote the formation of larger, lower-energy grains. As shown in Fig. 3(b), the EBSD results (Confidence index, Inverse Pole Figure map, and Kernel Average Misorientation map) indicate microstructural evolution after heat treatment. The IPF maps reveal an increase in Ni grain size, with the average grain size increasing from 0.598 μm to 0.874 μm. In addition, the KAM maps exhibit an overall decrease in local misorientation (0.584 to 0.400°), suggesting reduced local lattice distortion and stored strain. Taken together, these EBSD observations support that heat treatment promotes grain growth and recovery, leading to relaxation of residual/internal stress in the electrodeposited Ni layer. Unlike previous annealing studies on Ni-coated steel that discussed corrosion-related surface modification and passive-layer behavior, this study focused on post-plating heat treatment under an Ar atmosphere to suppress oxidation and examine the microstructural recovery of the Ni strike layer itself [13].

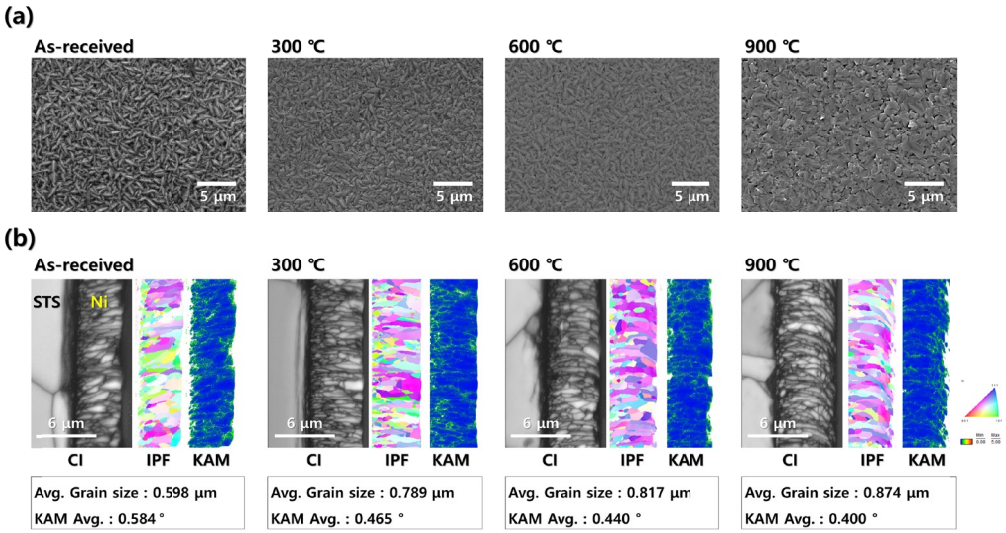

Fig. 3. Microstructural evolution of the Ni strike layer after heat treatment: (a) top-view SEM images of the as-deposited and heat-treated samples, and (b) EBSD results including confidence index (CI), inverse pole figure (IPF), and kernel average misorientation (KAM) maps for the as-deposited and heat-treated Ni layers

The heat-treated layer showed grain coarsening and a decrease in local misorientation, suggesting recovery and relaxation of residual/internal stress. These changes may be favorable for electrical conductivity and for maintaining a stable interlayer during subsequent plating, although measurements of electrical and adhesion properties were not included in the present study.

4. Conclusions

Nickel strike electrodeposition on stainless steel under potentiostatic control showed that the applied potential strongly affects not only the deposition rate, but also the balance between Ni reduction and competitive hydrogen evolution, which ultimately determines coating quality. As the applied potential became more negative from –0.9 to –1.8 V vs. Ag/AgCl, the cathodic current density increased and the current transient curves exhibited larger fluctuations, indicating intensified hydrogen evolution. Although the measured Ni-layer thickness increased from 4.6 to 10.3 μm with increasing overpotential, the current efficiency decreased from 22.3% to 10.8%, and non-uniform deposition with incomplete coating regions appeared at –1.8 V. These results indicate that excessively negative potentials accelerate apparent deposition, but simultaneously promote hydrogen-induced surface instability, thereby lowering deposition efficiency and degrading coating uniformity.

Under the more stable condition of –0.9 V, the Ni layer thickness increased linearly with deposition time, with an average growth rate of approximately 0.47 μm/min. Post-plating heat treatment transformed the as-deposited needle-like morphology into polygonal grains and promoted grain coarsening. EBSD analysis showed that the average grain size increased from 0.598 to 0.874 μm, while the KAM value decreased from 0.584 to 0.400°, indicating microstructural recovery and relaxation of residual/internal stress in the Ni strike layer. Overall, this study demonstrates that controlling hydrogen evolution during Ni strike plating is essential for achieving uniform and efficient coating formation, while subsequent heat treatment plays an important role in stabilizing the deposit microstructure. These findings provide a useful basis for optimizing Ni strike layers for reliable interfacial conditioning and subsequent plating processes.

Acknowledgments

This work was supported by the Materials & Components Technology Development Program, funded by the Ministry of Trade, Industry & Energy, 0Republic of Korea, and administered by the Korea Evaluation Institute of Industrial Technology (KEIT) (No. RS-2024-00431714)

REFERENCES

[1] A.D. Pingale, A. Owhal, A.S. Katarkar, S.U. Belgamwar, J.S. Rathore, Recent researches on Cu-Ni alloy matrix composites through electrodeposition and powder metallurgy methods: A review. Mater. Today Proc. **47** (11), 3301-3308 (2021). DOI: https://doi.org/10.1016/j.matpr.2021.07.145

[2] N.S. Mbugua, M. Kang, Y. Zhang, N.J. Ndiithi, G.V. Bertrand, L. Yao, Electrochemical Deposition of Ni, NiCo Alloy and NiCo–Ceramic Composite Coatings A Critical Review. Materials. **13** (16), 3475-3505 (2020). DOI: https://doi.org/10.3390/ma13163475

[3] V.N. Kale, S. Kumaraguru, G. Saravanan, A.S. Jalaluddeen, P. Rajkumar, R. Subadevi, M. Sivakumar, R.M. Gnanamuthu, Influence of nickel strike as adhesive layer on electrodeposited Zn-Co-Ni alloy and their performance in metalfinishing. Mater. Today Proc. **40**, S248-S253 (2021). DOI: https://doi.org/10.1016/j.matpr.2020.11.157

[4] A. Lelevic, F.C. Walsh, Electrodeposition of Ni-P alloy coatings: A review. Surf. Coat. Technol. **369**, 198-220 (2019). DOI: https://doi.org/10.1016/j.surfcoat. 2019.03.055

[5] M. Alper, H. Kockar, M. Safak, M.C. Baykul, Comparison of Ni–Cu alloy films electrodeposited at low and high pH levels. J. Alloys Compd. **453** (1-3), 15-19 (2008). DOI: https://doi.org/10.1016/j.jallcom.2006.11.066

[6] A. Karimzadeh, M. Aliofkhazraei, F.C. Walsh, A review of electrodeposited Ni-Co alloy and composite coatings: Microstructure, properties and applications. Surf. Coat. Technol. **372** (25), 463-498 (2019). DOI: https://doi.org/10.1016/j.surfcoat.2019.04.079

[7] F.S. Rudy, Surface preparation of various metals and alloys before plating and other finishing applications. Metal Finish. **105** (10), 147-162 (2007). DOI: https://doi.org/10.1016/s0026-0576(07)80329-1

[8] Y. Kamimoto, et al., Nickel-carbon composite plating using a Watts nickel electroplating bath. SN Appl. Sci. **2**, 1-6 (2020). DOI: https://doi.org/10.1007/s42452-020-1991-1

[9] E. Sezer, B. Ustamehmetoğlu, R. Katirci, Effects of functional groups of triple bonds containing molecules on nickel electroplating. Turk. J. Chem. **38** (5), 701-715 (2014). DOI: https://doi.org/10.3906/kim-1309-63

[10] A. Boukhouiete, Boumendjel, et al., Effect of current density on the microstructure and morphology of the electrodepositednickel coatings. Turk. J. Chem. **45** (5), 1599-1608 (2021). DOI: https://doi.org/10.3906/kim-2102-46

[11] J.G.D.R.D. Costa, C.L.F.D. Rocha, L.R.P.D.A. Lima, D.V. Ribeiro, C.A.C.D. Souza, Study of glycerol as an additive in Ni-Mo electrodeposition. Mater. Res. **25**, 139- 151 (2021). DOI: https://doi.org/10.1590/1980-5373-mr-2021-0139

[12] M. Miyagawa, K. Koshiba, J. Takahashi, K. Tatsumi, A New Method of Bonding SUS304 Stainless Steels Using Nickel-Iron Alloy Plating and Evaluation of the Mechanical Properties of the Bonds. ISIJ Int. **65** (13), 2235-2241 (2025). DOI: https://doi.org/10.2355/isijinternational.isijint-2025-227

[13] A.A. Dastgerdi, E. Rahimi, et al., The effect of combined annealing and temperrollingtreatments on the microstructure and corrosion properties of nickel electroplated coating. Appl. Surf. Sci. **709**, 163695-163709 (2025). DOI: https://doi.org/10.1016/j.apsusc.2025.163695